Three-Dimensional Computation of Toroidal Two-Fluid Internal Kink

C. R. Sovinec, E. C. Howell,
and P. Zhu
University of Wisconsin-Madison

2009 International Sherwood Fusion Theory Conference

Denver, Colorado May 3-5, 2009

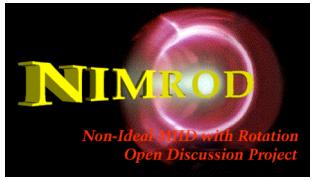

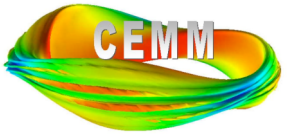

Outline

- Introduction
- Two-fluid computation
- Internal kink results
  - Comparison with MHD
  - Small vs. large *R/a*
  - Toroidal
- Conclusions

Introduction

Sawtooth activity is common among tokamaks with q=1 resonance, but theoretical understanding is incomplete.

- The source of free energy is described by resistive MHD; tokamak profiles with $q(0)<1$ are unstable.
- The fast crash is not produced by MHD with resistive reconnection.
  - Two-fluid reconnection may model the crash, but nonlinear 3D results are needed.
- Low $q(0)$ and incomplete reconnection have been observed.
  - Fast particle effects are significant.
- Our present focus is on the fast crash from two-fluid effects.

Previous nonlinear two-fluid 1/1 computations have assumed helical symmetry in a cylindrical geometry.

- Aydemir first compared linear behavior from Hazeltine's 4-field model with those of more complicated models [PFB **3**, 3025].
- His nonlinear computation with the same model predicted increasing $d\ln(E_k)/dt$ in the nonlinear stage [PFB **4**, 3469].
- Wang and Bhattacharjee developed an analytical model that predicts temporary finite-time singular behavior in island width [PRL **70**, 1627].
- Ottaviani and Porcelli considered large Δ' reconnection in a 2D slab with a reduced incompressible model [PoP **2**, 4104].
- Lukin reproduced Aydemir's result using incompressible, helically symmetric computations with hyper-resistivity [dissertation, Princeton, 2007].
- Germaschewski finds the same type of fast reconnection behavior from a full model [presentation GI1.00004, APS-DPP 2008].
- Computations described here are 3D and are both cylindrical and toroidal.

Two-Fluid Computation

- We solve a 'full' fluid-based system for low-frequency dynamics with the NIMROD code (http://nimrodteam.org).
- Computations solve linear and nonlinear initial-value problems.
- There are basis-function expansions for n, $\mathbf{V}$, $\mathbf{B}$, and T (or T_i and T_e).

$$\rho\left(\frac{\partial \mathbf{V}}{\partial t}+\mathbf{V}\cdot\nabla\mathbf{V}\right)=\mathbf{J}\times\mathbf{B}-\nabla p-\nabla\cdot\Pi_i(\mathbf{V})$$ flow evolution

$$\Pi_i=-\rho\nu_{kin}\nabla\mathbf{V}-\rho\nu_{iso}\mathbf{W}\,,\quad \mathbf{W}=\nabla\mathbf{V}+\nabla\mathbf{V}^T-\frac{2}{3}\mathbf{I}\nabla\cdot\mathbf{V}$$ ion stress models used here

$$\frac{\partial n}{\partial t}+\nabla\cdot(n\mathbf{V})=\nabla\cdot\left(D\nabla n-D_h\nabla\nabla^2 n\right)$$ particle continuity with artificial diffusivity

$$\frac{n}{\gamma-1}\left(\frac{\partial T_\alpha}{\partial t}+\mathbf{V}_\alpha\cdot\nabla T_\alpha\right)=-p_\alpha\nabla\cdot\mathbf{V}_\alpha-\nabla\cdot\mathbf{q}_\alpha+Q_\alpha$$ temperature evolution

$$\frac{\partial \mathbf{B}}{\partial t}=-\nabla\times\left[\eta\mathbf{J}-\mathbf{V}\times\mathbf{B}+\frac{1}{ne}(\mathbf{J}\times\mathbf{B}-T_e\nabla n)+\mu_0 d_e^2\frac{\partial \mathbf{J}}{\partial t}\right]+\kappa_{divb}\nabla\nabla\cdot\mathbf{B}$$ Faraday's / Ohm's law with divergence diffusion

$$\mu_0\mathbf{J}=\nabla\times\mathbf{B}$$ Ampere's law

NIMROD solves this system of equations with a numerical 'implicit leapfrog' algorithm [J. Phys: Conf. Series **16**, 25 (2005)].

- A plane (poloidal) of 2D spectral elements and finite Fourier series in the periodic coordinate (toroidal angle) allow spectral convergence.
- Implicit advances require solution of large algebraic systems at each step.
  - With symmetric geometry and equilibria, linear computations solve a separate linear system for each Fourier component, like separate 2D computations.
  - Matrices for nonlinear 3D computations have matrix elements that couple different Fourier components. They are <u>smaller</u> than the matrix elements for the poloidal-plane coupling <u>by at least one factor of the perturbation amplitude</u>.
  - Krylov-space solvers iterate with matrix-vector product operations but not elements of the matrix. Approximations of the matrices are used to accelerate or 'precondition' the iterations.

Hall-MHD in 3D has been problematic, because fluctuations do not contribute to the diagonal of our implicit **B**-advance operator, and the whistler is the fastest mode of the system.

- With **A** being a test function and dropping surface terms,

$$-\frac{\Delta t}{2}\int \mathbf{A}\cdot\nabla\times\left(\frac{1}{\mu_0\bar{n}e}\tilde{\mathbf{B}}^{j+1/2}\times\nabla\times\Delta\mathbf{B}\right)dVol =$$

$$-\frac{\Delta t}{2}\int \frac{1}{\mu_0\bar{n}e}(\nabla\times\mathbf{A})\cdot\tilde{\mathbf{B}}^{j+1/2}\times(\nabla\times\Delta\mathbf{B})\,dVol$$

- When the test and trial functions are expanded, the resulting matrix has mixed partials on the diagonal due to the cross product.
- With a Fourier expansion, the first-order toroidal derivatives lead to imaginary terms on the diagonal.
  - The operator is non-Hermitian.
  - It detracts from diagonal dominance when $\tilde{\mathbf{B}}^{j+1/2}$ and Δt are sufficiently large.

We have found that even at physical m_e/m_i ratios, implicit electron inertia helps matrix condition numbers.

• The HPD part of our system is increased by adding the $\frac{1}{\varepsilon_0 \omega_e^2}\frac{\partial}{\partial t}\mathbf{J}$ part of electron inertia.

$$\Delta\mathbf{B} - \frac{\Delta t}{2}\nabla\times\left(\mathbf{V}^{j+1}\times\Delta\mathbf{B}\right) + \frac{\Delta t}{2}\nabla\times\frac{1}{\bar{n}e}\left(\mathbf{J}^{j+1/2}\times\Delta\mathbf{B} + \Delta\mathbf{J}\times\mathbf{B}^{j+1/2}\right)$$

$$+\Delta t\,\nabla\times\left(\frac{\eta}{2} + \frac{d_e^2}{\Delta t}\right)\nabla\times\Delta\mathbf{B} - \Delta t\,\kappa_{divb}\nabla\nabla\cdot\Delta\mathbf{B}$$

for the lhs of the **B**-advance, also showing the divergence cleaning term. The electron skin depth is $d_e = c/\omega_e$.

• Through polarization drift, electron inertia leads to the electron cyclotron resonance, which keeps the *R*-mode phase speed from growing without bound as k_{max} increases with spatial resolution.

• This helps limit stiffness, hence condition numbers, in two-fluid computations.

Fourier coupling in the preconditioner for non-Hermitian (2-fluid) systems is critical for 3D computations.

- Limited coupling of Fourier components is used in a new preconditioner.
- It is designed for increasing use of parallelism, available in new multi-core massively parallel computers, to achieve resolution in global computations.

- Scaling study is a two-fluid kink in the early nonlinear stage; $\Delta t = 0.1\ \tau_A$.
- Results are from the Cray XT4 at NERSC ("Franklin"), quad-core.
- Parameters provide a weak scaling of a production computation.
- New preconditioner help keep GMRES iterations fixed with increasing N_{Four}.
- The largest computation has 1.8×10^8 degrees of freedom (coefficients of the high-order representation) and exceeds the 1-TFlop level of actual performance.

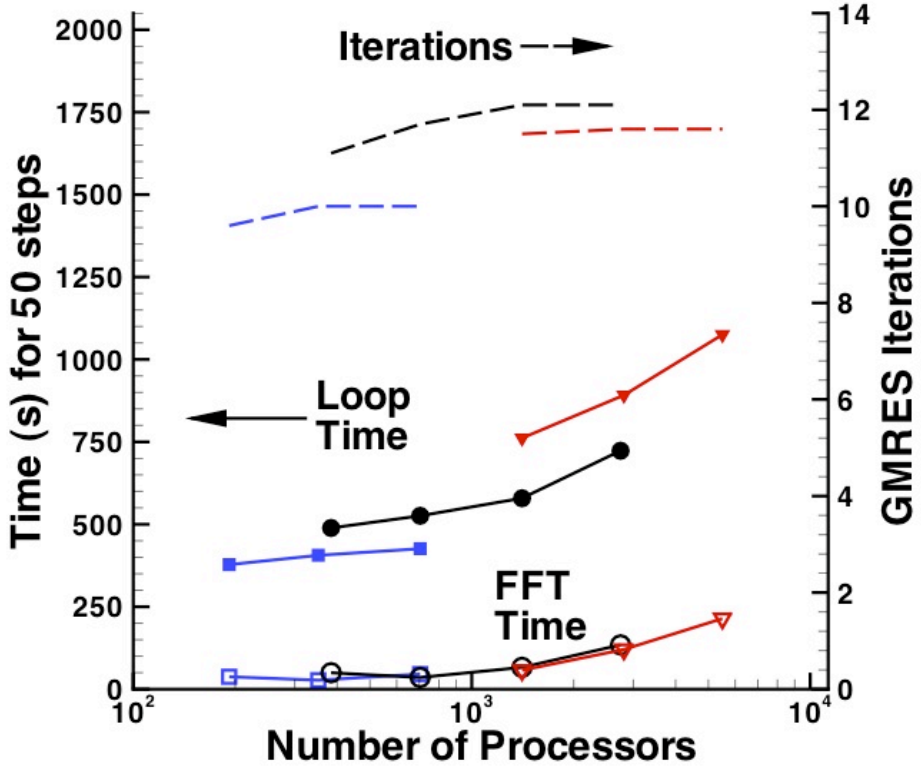

Blue: 32 blocks; Black: 64 blocks; Red: 128 blocks. Within color shows increasing N_{Four}.

Internal Kink Results: Parameters are chosen for comparison with the published 2D results.

- We consider circular cross-section tori (R/a=4) and cylinders ($1 \le R/a \le 4$) with equilibrium profiles that are similar to the Aydemir computation.
- The pressure is flat, so there are no equilibrium diamagnetic effects.
- Our computations use the following plasma parameters:

$$S = \tau_r / \tau_{Hp} = 10^6 \quad \tau_r \equiv \mu_0 a^2 / \eta \quad \tau_{Hp} \equiv a\sqrt{\mu_0 \rho}/B_p$$

$$\beta = 5\times 10^{-3} \quad \delta = d_i/2 = 0.11 \quad \left(d_\alpha \equiv c\sqrt{\frac{\varepsilon_0 m_\alpha}{n_\alpha q_\alpha^2}} \right) \quad \rho_s = 1.5\times 10^{-2} \quad d_e = 5\times 10^{-3}$$

$$\mu_0 \nu_{iso}/\eta = \mathrm{Pm} = 0.1 \quad T_i \cong 0$$

- Computations use hyper-particle-diffusivity to avoid numerical noise in the particle density, $\mu_0 D_h / \eta a^2 = 10^{-4}$.
- In the cylindrical cases, $q(r)$=0.98+0.51$(r/a)^2$, and the 1/1 resonant surface is at r=0.2a.
  - B_z is scaled with R/a to keep the same S-value (approximately).
  - Poloidal-β then varies with R/a:

$$\beta_{pol} = \beta(R/r_s)^2 = 1/8 \text{ at } R/a = 1, \quad 1/2 \text{ at } R/a = 2, \quad 2 \text{ at } R/a = 4$$

Linear resistive-MHD computations indicate that the cylinder modes are resistive at S=10^6 and *R/a*=4 and ideal at *R/a*=1.

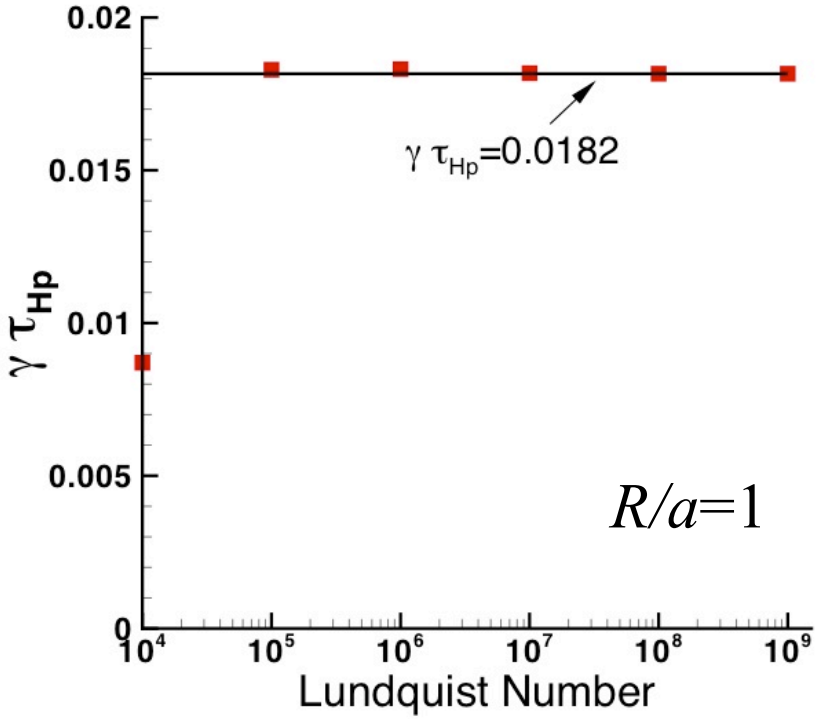

- At *R/a*=1, growth-rates are independent of S, except at small S.
- At small S-value, the mode is damped and overstable.
- The eigenfunction at S=10^6 indicates little reconnection.

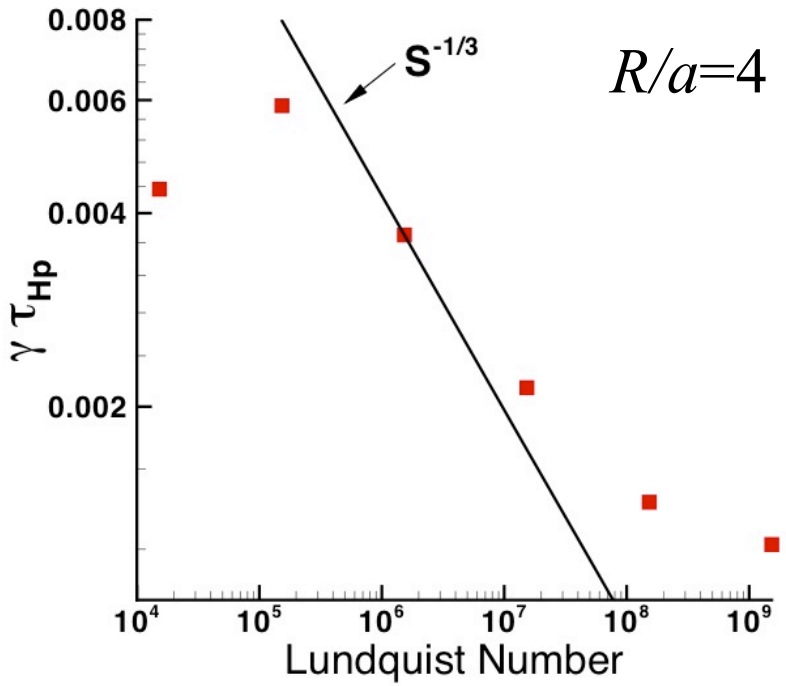

- There is a narrow range where growth-rates follow $S^{-1/3}$ scaling.
- At smaller S-values, the mode is damped.
- At S>10^9, the growth-rate approaches a constant (ideal) value with virtually no *B*-normal at the *q*=1 surface.

There are no diamagnetic effects in this equilibrium, and two-fluid linear growth rates are slightly larger than resistive MHD results.

- The aspect ratio (hence β_p) has a greater effect on linear growth rates.

R/a	S	$\gamma_{MHD}\tau_{Hp}$	$\gamma_{2fl}\tau_{Hp}$
1	1.0×10^{6}	1.83×10^{-2}	2.07×10^{-2}
2	1.39×10^{6}	5.59×10^{-3}	6.71×10^{-3}
4	1.53×10^{6}	3.64×10^{-3}	4.37×10^{-3}

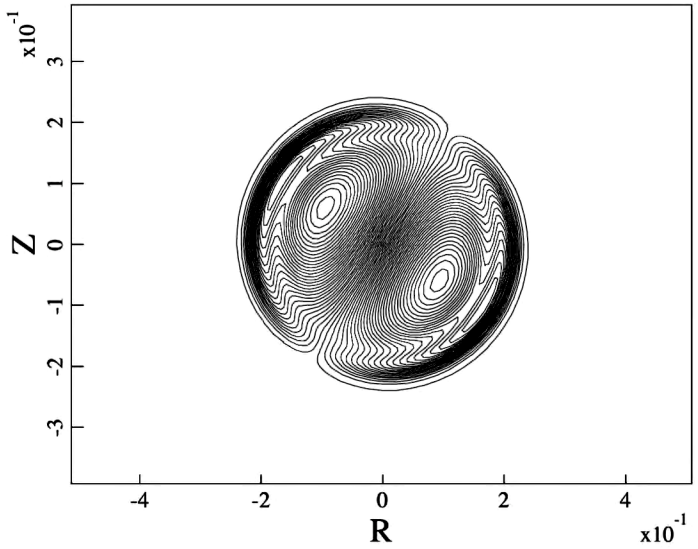

Axial flow velocity, rMHD, R/a=2.

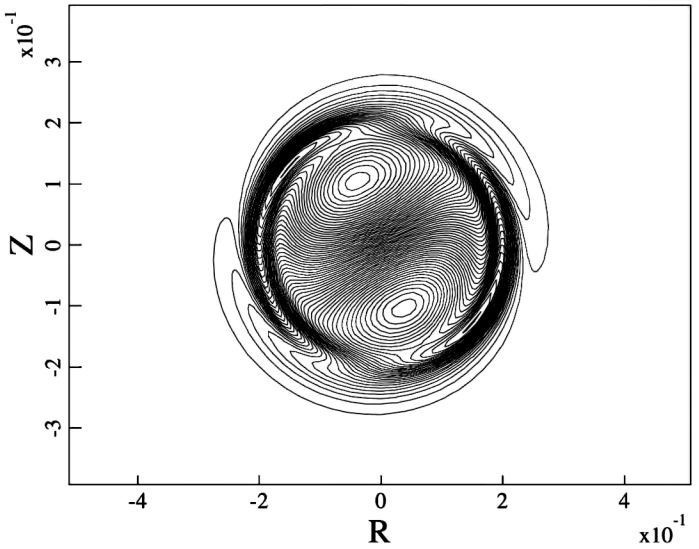

Axial flow velocity, 2fl, R/a=2.

For this cylindrical equilibrium, the nonlinear 'growth-rate' increase reported by Aydemir is observed at large R/a.

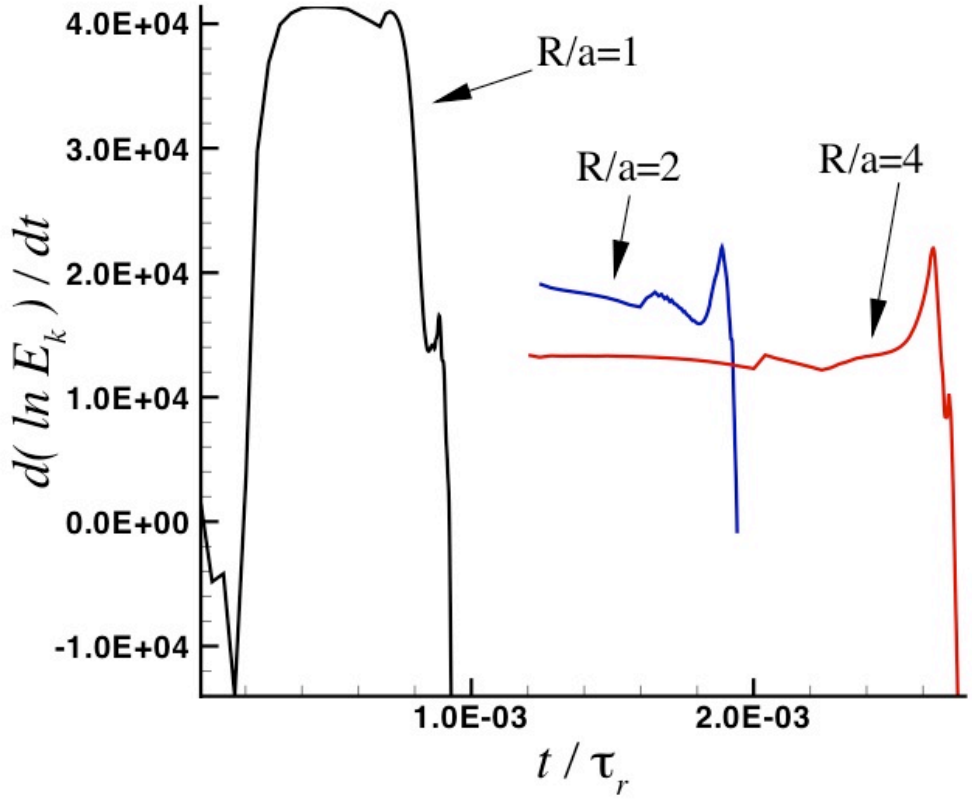

- Degree of polynomials is 8; $0 \le n \le 85$ for $R/a=1$ and $0 \le n \le 42$ for others.
- Although the NIMROD computations are 3D, the evolution appears to remain helically symmetric in all cylindrical cases--no secondary modes.

Poincaré surfaces of the cylindrical R/a=4 two-fluid results show steady island growth before γ_{nl} increases.

Island is ~5% at t=3651 τ_{Hp}

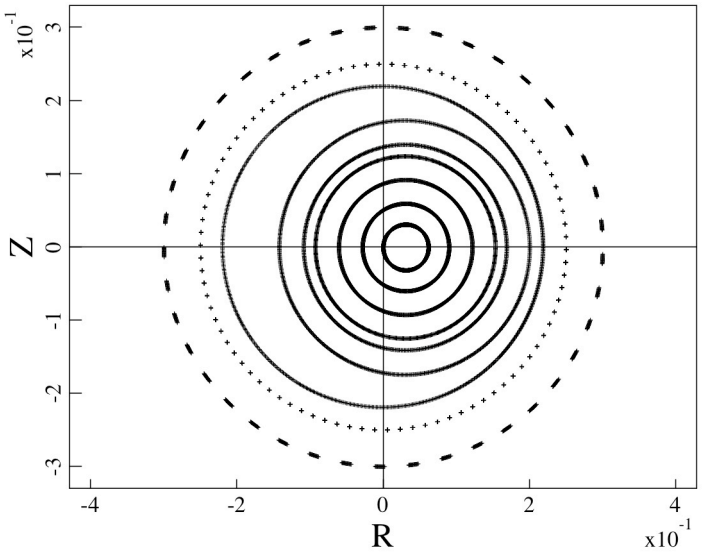

t=3830 τ_{Hp}

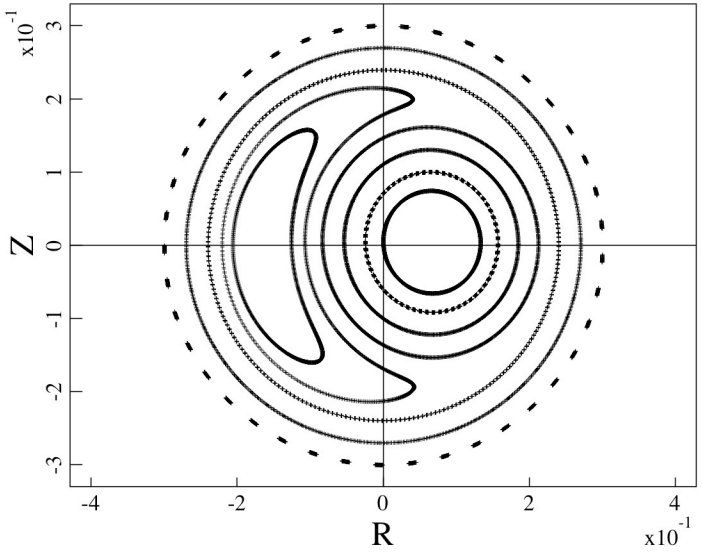

Time of peak n=1 energy, start of increasing γ_{nl} , t=3911 τ_{Hp}

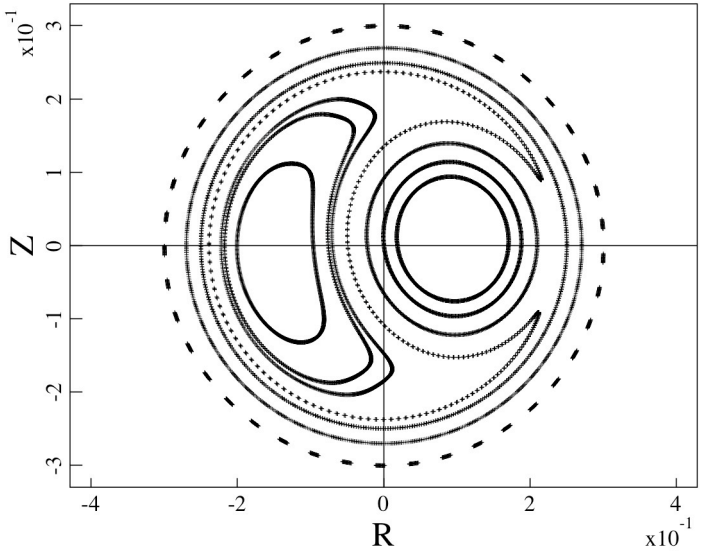

Peak γ_{nl} t=4024 τ_{Hp}

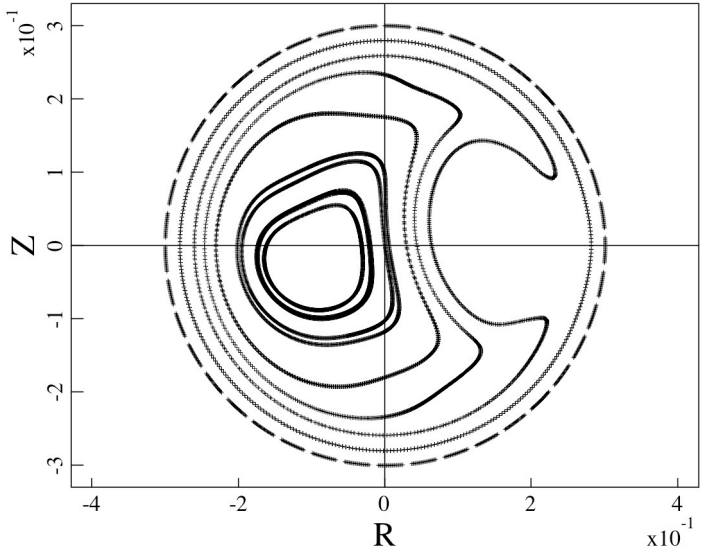

Poincaré surfaces of the ideally unstable cylindrical R/a=1 two-fluid results appear more MHD-like.

Island is ~10% at t=806 τ_{Hp}

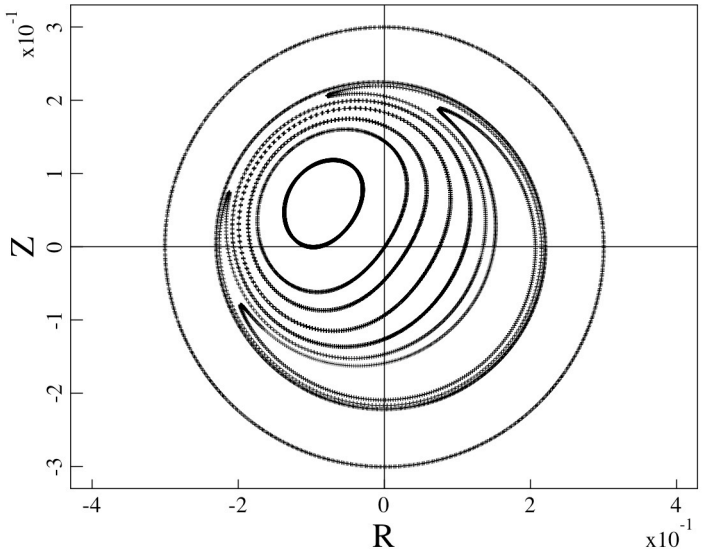

decreasing γ_{nl} , t=844 τ_{Hp}

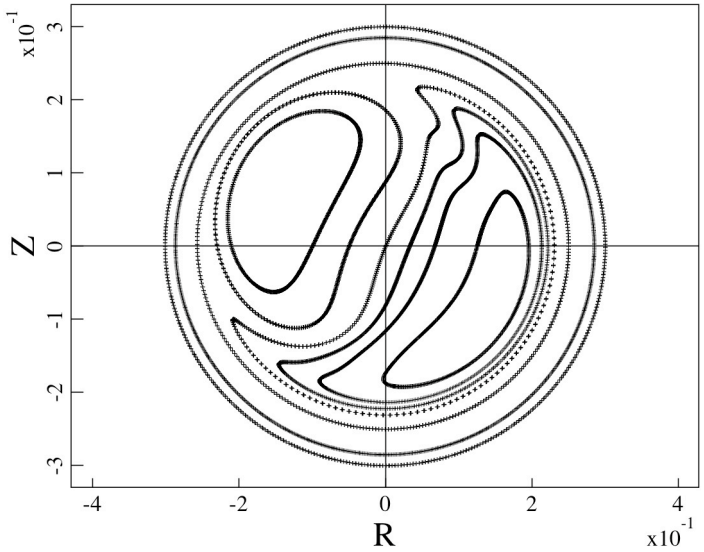

Time of peak n=1 energy, t=858 τ_{Hp}

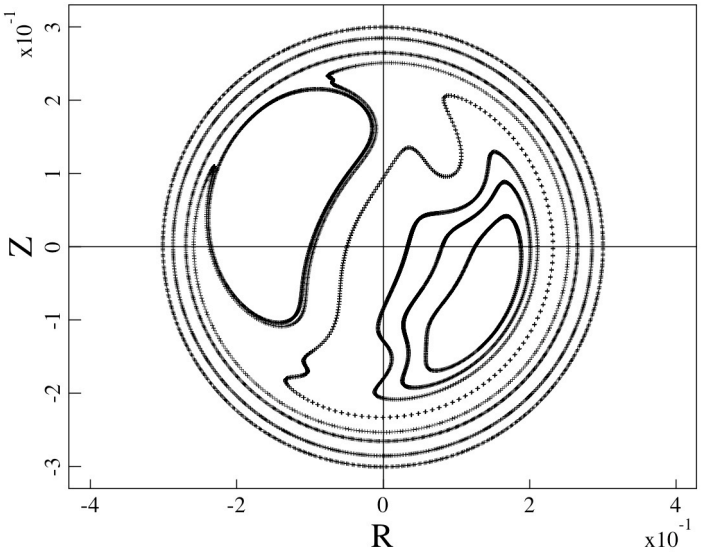

Blip in γ_{nl} t=882 τ_{Hp}

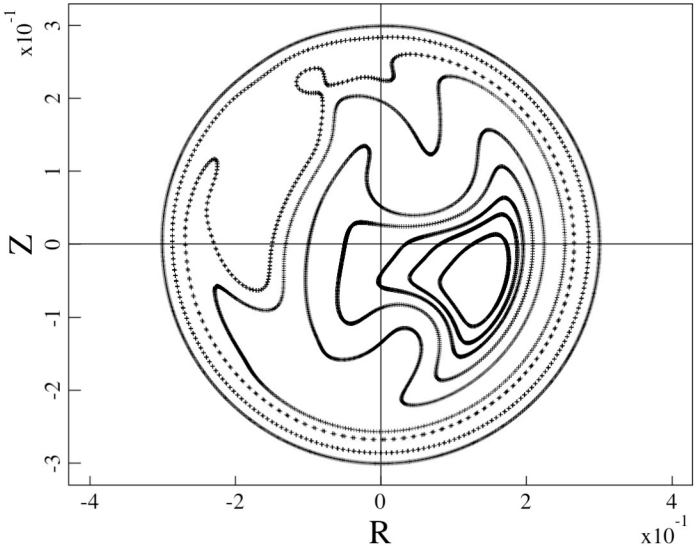

Poincaré surfaces from a cylindrical R/a=1 computation with MHD maintain Y-type reconnection geometry.

Island is ~10% at t=916 τ_{Hp}

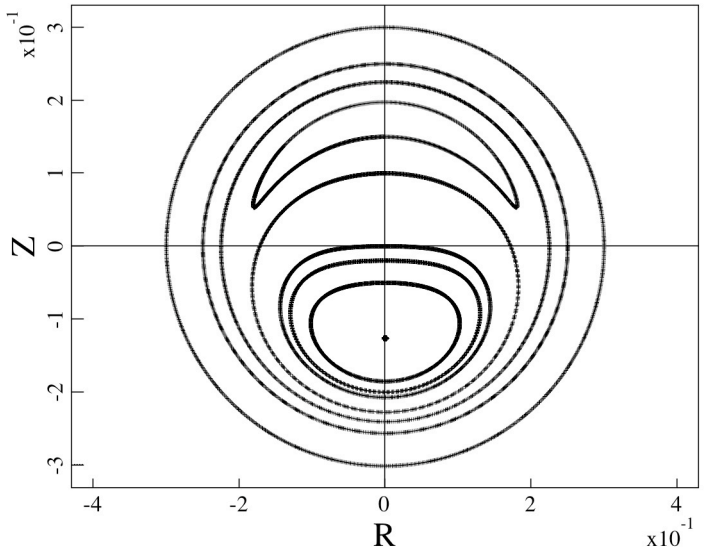

t=941 τ_{Hp}

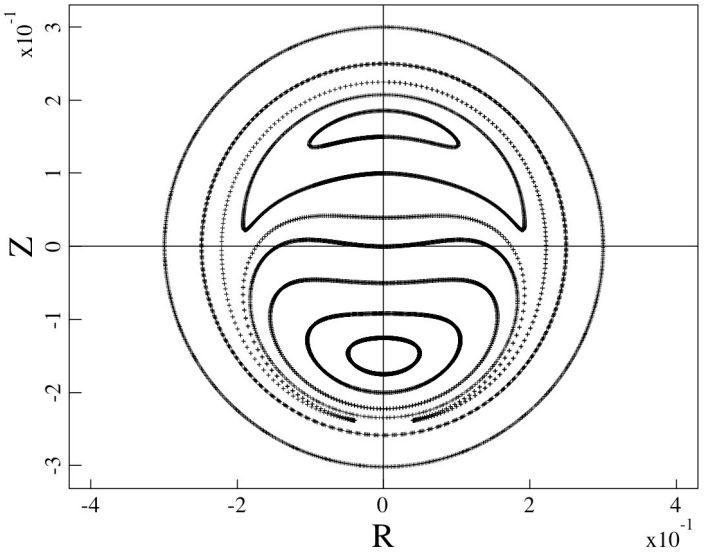

Peak n=1 energy at t=983 τ_{Hp}

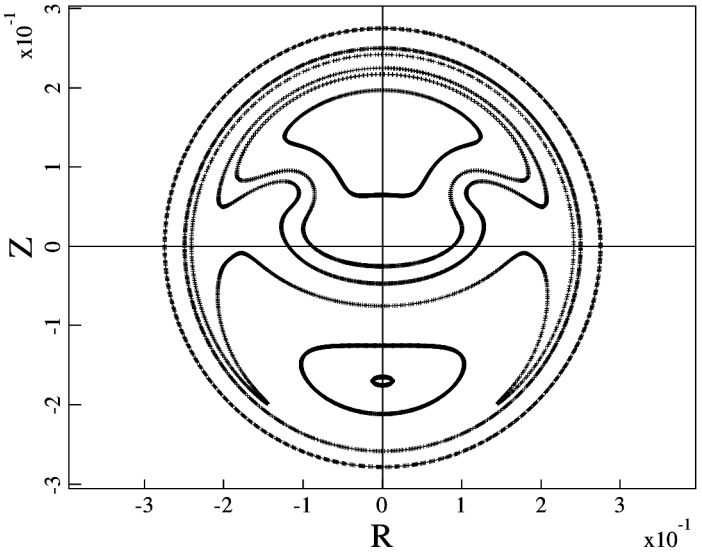

Reconnection completing at t=1137 τ_{Hp}.

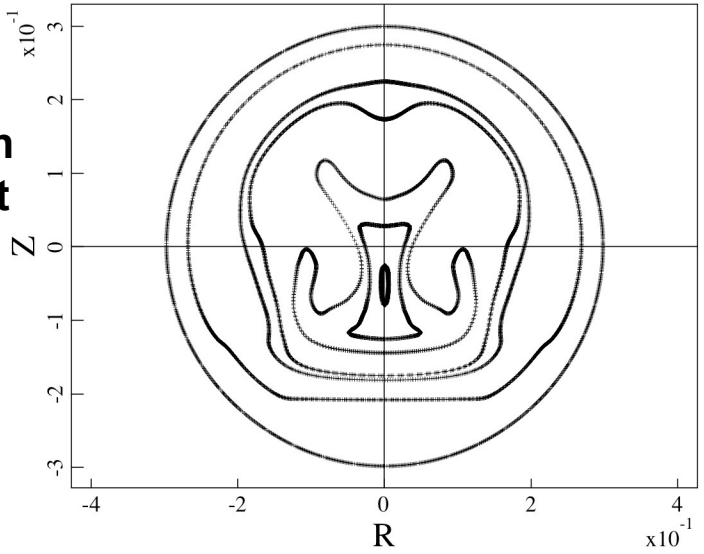

Magnetic fluctuation energy traces show a somewhat distinguishable crash only in the two-fluid *R/a*=1 case.

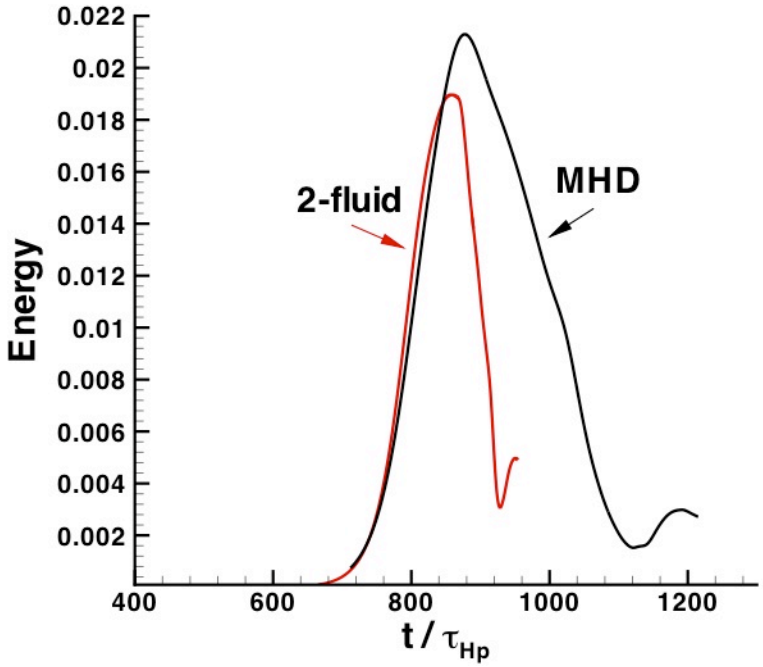

Magnetic n=1 fluctuation energies from two-fluid and MHD computations at *R/a*=1. The two-fluid crash in energy occurs in 60 τ_{Hp}.

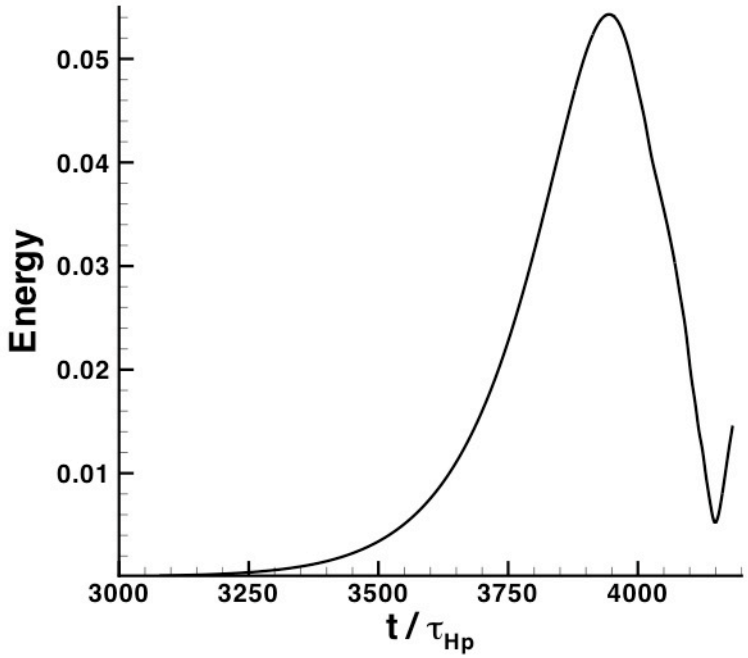

Magnetic n=1 fluctuation energy from the two-fluid computation with *R/a*=4.

The relative importance of two different effects needs to be understood:

- Ideal vs. resistive linear instability
- Poloidal-β below or above unity

The importance of β and possibly ideal instability may be inferred from the fluid-model plane-wave dispersion relation with massless electrons and cold ions.

• Using frequency normalized by Ω_i, lengths normalized by ion skin-depth (i.e. Alfvén wave is $\omega^2=k^2$):

$$\omega^4 K^2 - \omega^2\left\{\left(k^2+K\right)\left(k_{||}^2+K\right)+\beta\left[K\left(k_\perp^2+Kk_{||}^2\right)+k_{||}^2k_\perp^2(1-K)^2\right]\right\}$$

$$+\beta k_{||}^2\left(k^2+K\right)\left(k_{||}^2+K+Kk_\perp^2\right)=0$$

where $K \equiv \omega^2/\left(\omega^2-1\right)$ reflects ion polarization vs. inertia and is $-\omega^2$ at $\omega^2 << 1$ and becomes unity at $\omega^2 >> 1$.

• The first (ω^4) term is only important for the fast wave.

• The dispersive KAW is critical for our two-fluid reconnection [Rogers, PRL **87**, 195004 (2001)] and is a balance between the second (ω^2) and third (ω^0) terms.

• Speculation: either 1) large β or 2) large $k_{||}$ may occur through plasma conditions or nonlinear ideal evolution, respectively.

Toroidal Geometry: Simulations of the internal kink in toroidal geometry investigate inherently 3D evolution.

- Equilibria are generated with the NIMEQ code.
- $R/a = 4$
- Plasma parameters are similar to the cylindrical computations:

$$S = \tau_r / \tau_{Hp} = 1.48 \times 10^6 \ , \ q(a) < 2 \text{ case}$$

$$S = 8.11 \times 10^5 \ , \ q(a) > 2 \text{ case}$$

$$\tau_{Hp} \equiv 2\pi a^2 \sqrt{\mu_0 \rho} / \mu_0 I_p$$

$$d_e = 5 \times 10^{-3} \quad \delta = d_i / 2 = 0.11 \quad \rho_s = 1.5 \times 10^{-2}$$

$$\mu_0 \nu_{iso} / \eta = \mathrm{Pm} = 0.1 \quad T_i \cong 0$$

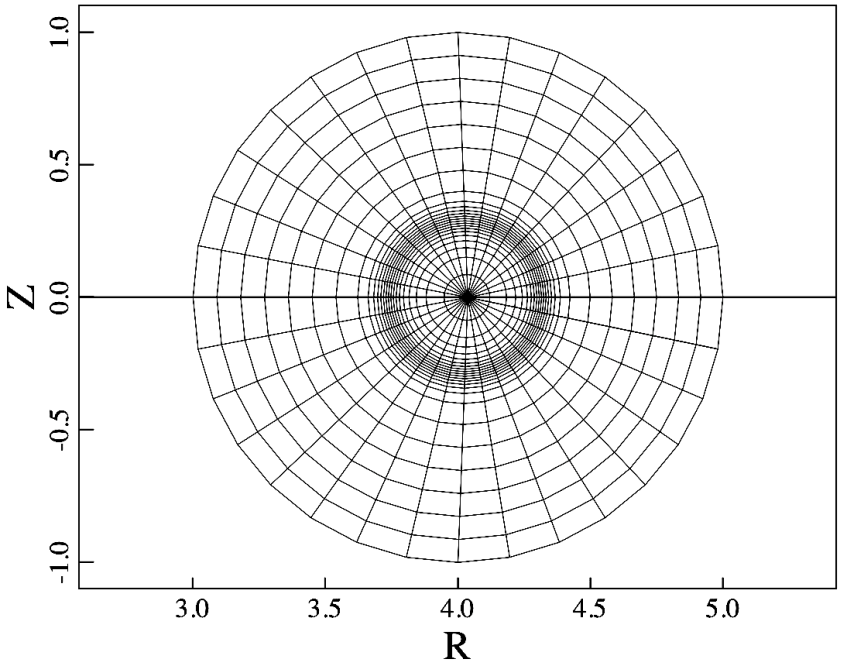

Mesh of spectral elements reflects slight Shafranov shift and is packed near 1/1 resonance.

The importance of a second rational surface is checked by considering two equilibria.

- Like the cylindrical computations, the pressure profile is uniform, and

  $\beta=5\times10^{-3}$

- For the first equilibrium,

  $F = 3.44 + 0.12(1-\psi) + 0.064\psi(\psi-1)$

  where ψ is the normalized ring flux.

- Here, $q(0)=0.97$, $q(a)=1.61$.

- For the second equilibrium,

  $F = 3.50 + 0.064(1-\psi) + 0.020\psi(\psi-1)$

- Here, $q(0)=0.97$, $q(a)=2.99$.

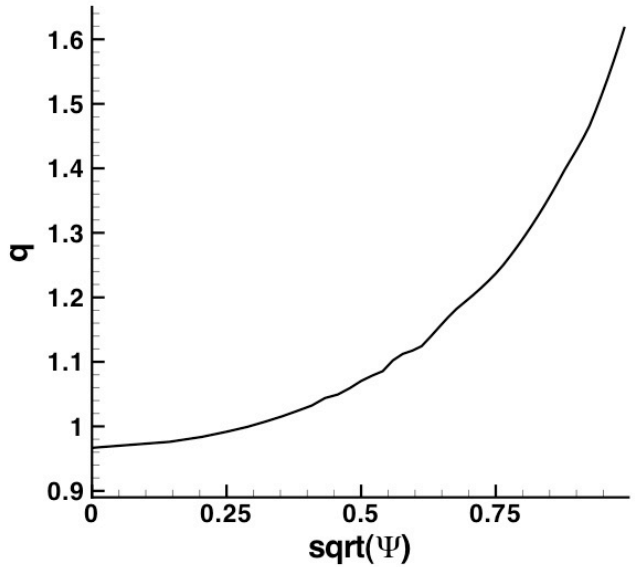

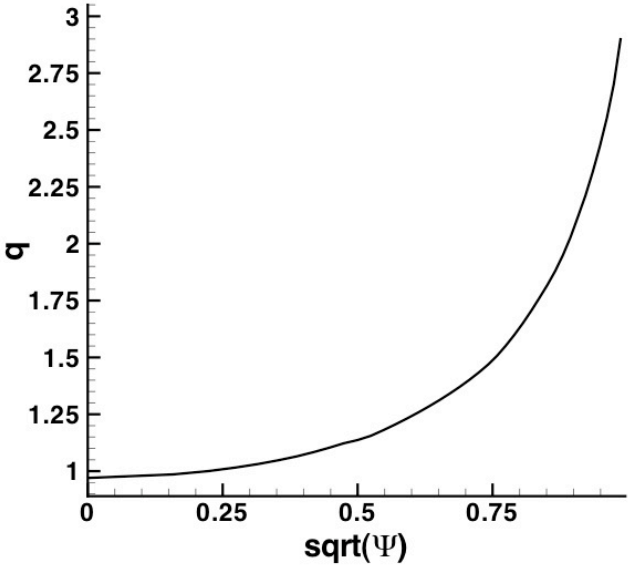

Moderate and high resolution computations obtain the nonlinearly increasing kinetic energy growth-rate.

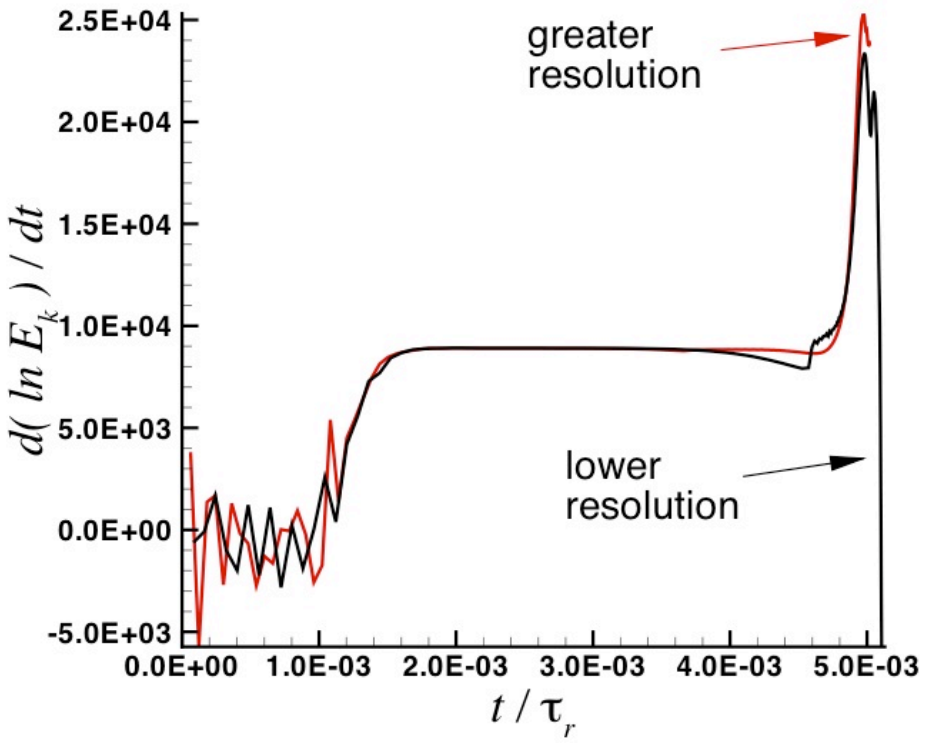

- First case has a 20×20 mesh, degree of polynomials is 8, and $0 \le n \le 42$.
- Second case has a 24×32 mesh, degree of polynomials is 8, and $0 \le n \le 85$.
- The moderate and large computations were run on 300 and 1376 cores of "Franklin" in quad-core configuration.

The toroidal computations show a clear X-point reconnection geometry when the growth-rate of kinetic energy increases.

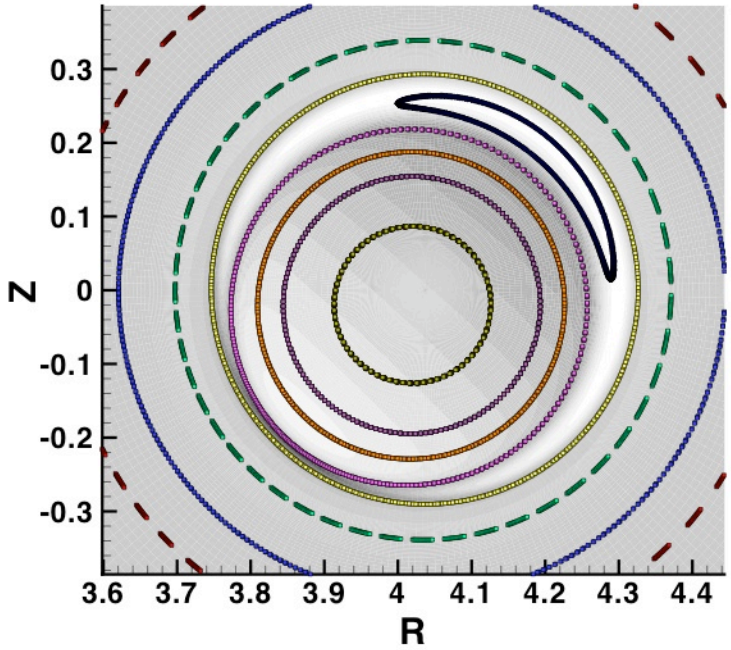

Just before the increase in growth rate (t=4.67×10^{-3} τ_r), there is a broad layer of parallel current density (grayscale) where field-lines are reconnecting.

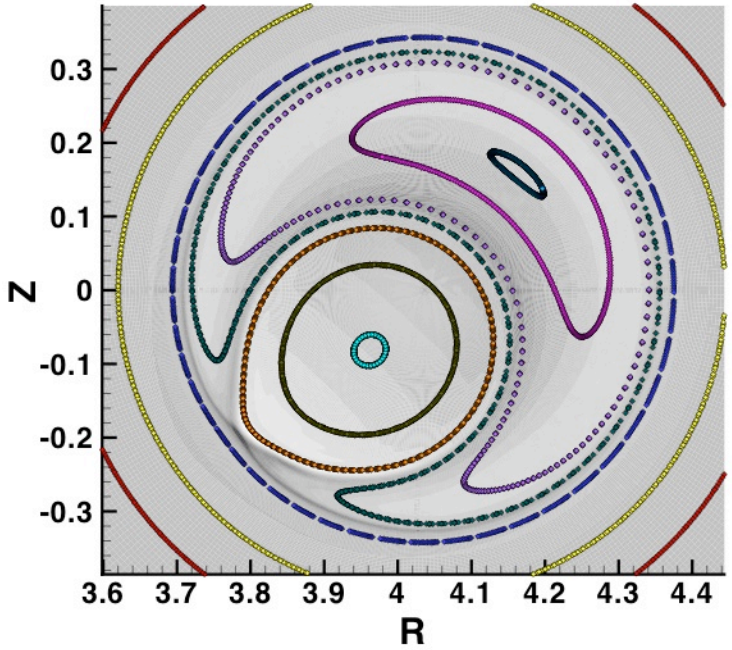

Near the peak growth rate (t=4.95×10^{-3} τ_r), x-point reconnection is evident, and parallel current is concentrated.

- While the toroidal cases are inherently 3D, initial R/a=4 results are qualitatively similar to helically symmetric cylindrical results.

The first crash of a $q(a)$=3 computation is qualitatively similar.

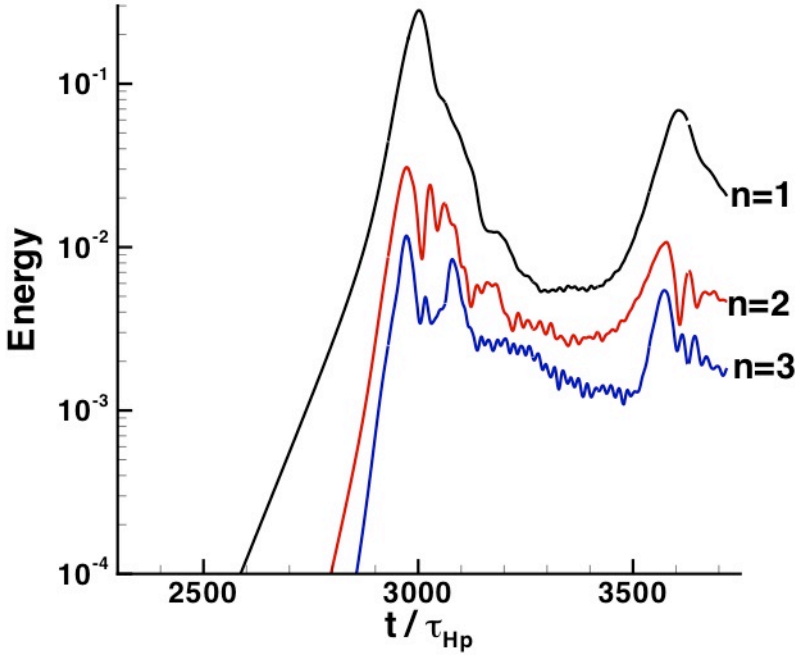

Selected kinetic fluctuation energies.

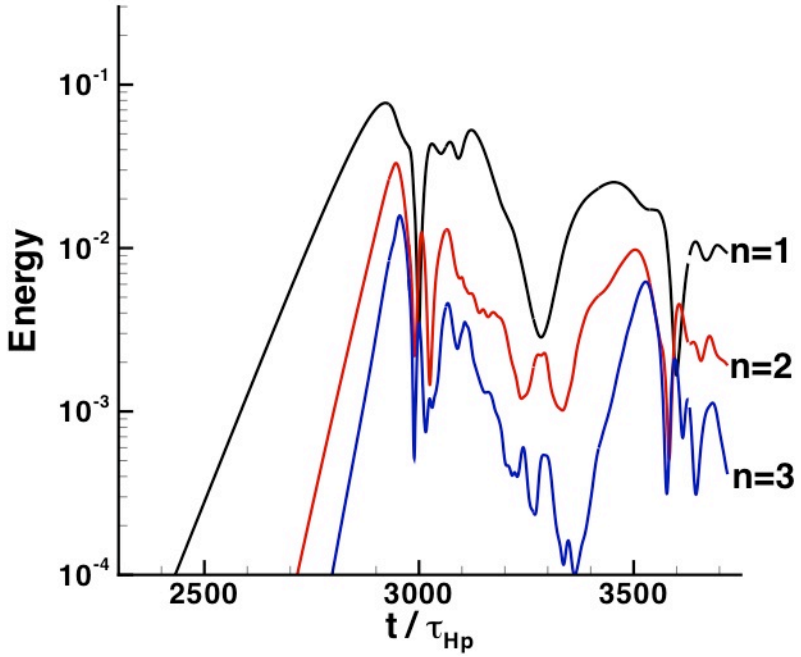

Selected magnetic fluctuation energies.

- Resolution is $0 \le n \le 42$; 24×32 mesh, degree of polynomials is 7.
- There is no appreciable coupling to the q=2 surface.
- The cycle period is short at ~600 τ_{Hp}; this computation does not include effects associated with thermal transport.

The n=0 profile returns to the original $q(0)$-value before the second crash.

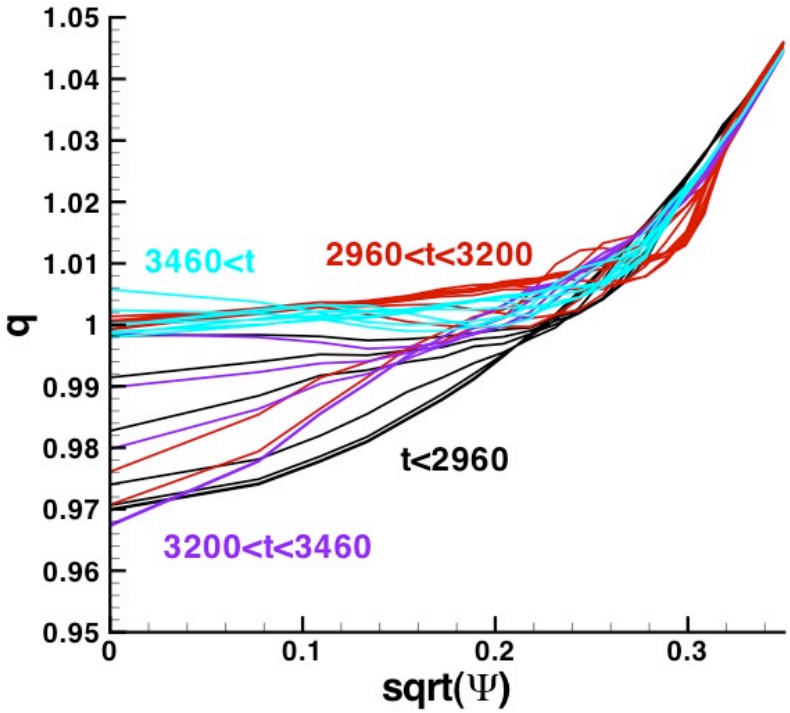

Evolution of the safety-factor profile for 1) pre-first crash, 2) through first crash, 3) pre-second crash, and 4) after second crash.

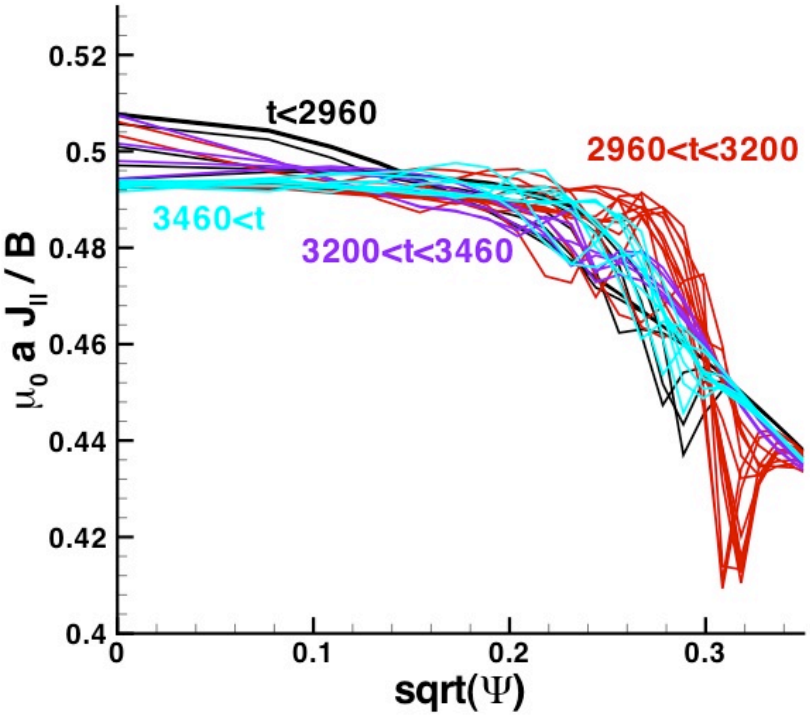

Evolution of parallel current density profile.

Conclusions

- Improvements to NIMROD's computational linear algebra are facilitating two-fluid macroscopic computation in 3D.
- Non-reduced 3D two-fluid results in a cylinder reproduce X-point reconnection and increasing kinetic-energy growth rate for large R/a.
- At small R/a, there is a more distinct crash with two-fluid effects.
- Toroidal geometry computations are inherently 3D, but initial two-fluid results are qualitatively similar to the cylindrical results.
- With these low-β equilibria, coupling to q=2 is not significant.